


Fixing effective range parameters in elastic α - ^{12}C scattering: impact on resonant 2_4^+ state of ^{16}O and S_{E2} factor of $^{12}\text{C}(\alpha, \gamma)^{16}\text{O}^*$

Shung-Ichi Ando[†] 

Department of Display and Semiconductor Engineering, and Research Center for Nano-Bio Science, Sunmoon University, Asan, Chungnam 31460, Republic of Korea

Abstract: Elastic α - ^{12}C scattering for $l=2$ and $E2$ transition of radiative α capture on ^{12}C and $^{12}\text{C}(\alpha, \gamma)^{16}\text{O}$ are studied in cluster effective field theory. Owing to the problem in fixing the asymptotic normalization coefficient (ANC) of the subthreshold 2_1^+ state of ^{16}O or, equivalently, the effective range parameters of the 2_1^+ state, from the elastic scattering data, we introduced the conditions that lead to a large value of the ANC in this study. We also introduced d -wave phase shift data of the elastic scattering up to the α energy, $E_\alpha = 10$ MeV, which contain the resonant 2_4^+ state of ^{16}O . Applying these conditions, the parameters of the S matrix of the elastic scattering for $l=2$ were fitted to the phase shift data, and the fitted parameters were employed in the calculation of the astrophysical S_{E2} factor of $^{12}\text{C}(\alpha, \gamma)^{16}\text{O}$; we extrapolated the S_{E2} factor to the Gamow-peak energy, $E_G = 0.3$ MeV. We found that the aforementioned conditions lead to significant effects in the observables of the 2_4^+ state of ^{16}O and the estimate of the S_{E2} factor at E_G and confirmed that the ANC of the 2_1^+ of ^{16}O cannot be determined by the phase shift data for $l=2$.

Keywords: radiative alpha capture on carbon-12, elastic alpha-carbon-12 scattering, astrophysical S factor for $E2$ transition, ANC of sub-threshold 2_+ state of oxygen-16, effective range expansion, cluster effective field theory

DOI: 10.1088/1674-1137/addaae

CSTR: 32044.14.ChinesePhysicsC.49094107

I. INTRODUCTION

The radiative α capture on ^{12}C and $^{12}\text{C}(\alpha, \gamma)^{16}\text{O}$ is one of the fundamental reactions in nuclear astrophysics. It determines, along with the triple α reaction, the C/O ratio in the core of a helium-burning star [1]. It also provides an initial condition for computer simulations of star evolution [2, 3] and significantly influences the results of star explosions and nucleosynthesis [4]. However, the reaction rate or, equivalently, the astrophysical S factor of $^{12}\text{C}(\alpha, \gamma)^{16}\text{O}$ at the Gamow-peak energy, $E_G = 0.3$ MeV, has not been measured in an experimental facility because of the Coulomb barrier. One needs to employ a theoretical model, fit the model parameters to experimental data measured at an energy scale of a few MeV, and extrapolate the reaction rate to E_G . Meanwhile, it is known that $E1$ and $E2$ transitions of $^{12}\text{C}(\alpha, \gamma)^{16}\text{O}$ are dominant owing to the subthreshold 1_1^- and 2_1^+ (I_{th}^π) states of ^{16}O , whose binding energies with respect to the α - ^{12}C breakup energy are $B_1 = 0.045$ MeV and $B_2 = 0.245$ MeV, respectively [5]. During the past half-century, many experiment-

al and theoretical studies on the reaction have been carried out. For a review, refer, *e.g.*, to Refs. [6–10] (for a brief review, see Ref. [11]).

We previously studied reactions related to $^{12}\text{C}(\alpha, \gamma)^{16}\text{O}$ by constructing a low-energy effective field theory (EFT) based on the methodology of quantum field theory [12–14]. When constructing an EFT, one first chooses a typical scale of a reaction to study and then introduces a large scale for relevant degrees of freedom at low energy to separate from irrelevant degrees of freedom from high energy. We chose the Gamow-peak energy, $E_G = 0.3$ MeV, as a typical energy scale; a typical momentum scale would be $Q = \sqrt{2\mu E_G} = 40$ MeV, where μ is the reduced mass of α and ^{12}C ¹⁾. Because the typical wavelength of the reaction is larger than the size of the nuclei, nucleons inside the nuclei would be irrelevant; we assigned α and ^{12}C as structure-less (point-like) spin-0 scalar fields. We then chose the energy difference between p - ^{15}N and α - ^{12}C breakup energies of ^{16}O ; $\Delta E = 12.13 - 7.16 = 4.97$ MeV, as the high energy (separation) scale; the high momentum scale was set as

Received 21 February 2025; Accepted 19 May 2025; Published online 20 May 2025

* Supported by the National Research Foundation of Korea (NRF) grant funded by the Korean government (MSIT) (2019R1F1A1040362, 2022R1F1A1070060, 2023R1A2C1003177) and the Korean Evaluation Institute of Industrial Technology (KEIT) grant funded by the Korean government (MOTIE) (20022473)

[†] E-mail: sando@sunmoon.ac.kr1) A typical length scale of the reaction is $Q^{-1} = 4.8$ fm.

©2025 Chinese Physical Society and the Institute of High Energy Physics of the Chinese Academy of Sciences and the Institute of Modern Physics of the Chinese Academy of Sciences and IOP Publishing Ltd. All rights, including for text and data mining, AI training, and similar technologies, are reserved.

$\Lambda_H = \sqrt{2\mu\Delta E} = 160$ MeV. The theory provides us with a perturbative expansion scheme featuring an expansion parameter of $Q/\Lambda_H = 1/4$. The p - ^{15}N system is now regarded to have irrelevant degrees of freedom and is integrated out of the effective Lagrangian, whose effects are embedded in the coefficients of terms of the Lagrangian. In principle, these coefficients can be determined from the mother theory; in practice, they are fixed by using experimental data or empirical values. Because of the perturbative expansion scheme of EFT, by truncating the terms up to a given order, one can obtain an expression of reaction amplitudes in terms of a few parameters for each of the reaction channels. This approach was recently used for the study of important reactions in nuclear astrophysics, such as elastic p - ^{12}C scattering [15], elastic d - α scattering [16], and radiative proton capture on ^{15}N [17, 18].

Previously, we studied various cases of elastic α - ^{12}C scattering at low energies [19–23], $E1$ transition of $^{12}\text{C}(\alpha, \gamma)^{16}\text{O}$, and an estimate of the S_{E1} factor of $^{12}\text{C}(\alpha, \gamma)^{16}\text{O}$ at E_G [24], as well as β delayed α emissions from ^{16}N [10] up to the sub-leading order within the cluster EFT. The experimental data of each of the reactions are well reproduced by the fitted values of the parameters of reaction amplitudes. However, we observed a problem in a previous study (see Fig. 6 in Ref. [22]): when applying the fitted parameters to the precise phase shift data up to the p - ^{15}N breakup energy, $E_\alpha = 6.62$ MeV (E_α is the α energy in the laboratory frame), reported by Tischhauser *et al.* (2009) [25], a path of the inverse of dressed ^{16}O propagator for $l=2$ cannot be uniquely determined in the low-energy region, where the S_{E2} factor is extrapolated to E_G . In this study, we analyzed this issue by introducing conditions applied to the effective range parameters in the low-energy region and by employing two types of experimental data: the phase shift of the elastic α - ^{12}C scattering explicitly including the resonant 2_4^+ state of ^{16}O and the S_{E2} factor of $^{12}\text{C}(\alpha, \gamma)^{16}\text{O}$ below the energy of sharp resonant 2_2^+ state of ^{16}O .

A known problem in the study of the elastic α - ^{12}C scattering for $l=2$ at low energy is that the asymptotic normalization coefficient (ANC) of the subthreshold 2_1^+ state of ^{16}O calculated from the effective range parameters is significantly smaller than the values deduced from other reactions, such as α transfer reactions. An estimate of the ANC of the subthreshold 2_1^+ state of ^{16}O , $|C_b|_2$, using the effective range parameters was reported by König, Lee, and Hammer to be $|C_b|_2 = (2.41 \pm 0.38) \times 10^4 \text{ fm}^{-1/2}$ [26], which is smaller by approximately a factor of five than the value of $|C_b|_2 = (1.11 \pm 0.11) \times 10^5 \text{ fm}^{-1/2}$ deduced from the α -transfer reactions, $^{12}\text{C}(^6\text{Li}, d)^{16}\text{O}$ and $^{12}\text{C}(^7\text{Li}, t)^{16}\text{O}$ [27]. Meanwhile, a large uncertainty of the ANC of the 2_1^+ state deduced from the elastic α - ^{12}C scattering within a potential model, with values ranging from 2 to $18 \times 10^4 \text{ fm}^{-1/2}$, was reported by Sparenberg, Capel, and Baye [28] (the values of the ANC for the

2_1^+ state of ^{16}O reported in literature are summarized in Table 2 in Ref. [29]). As will be discussed in the following, the inverse of the dressed ^{16}O propagator for $l=2$ is expressed in terms of the three effective range parameters, r_2 , P_2 , and Q_2 , which approximately configure a cubic polynomial function. Fig. 6 in Ref. [22] features three types of lines: 1) those having a maximum point and a minimum point, 2) those having a plateau, and 3) those simply decreasing, obtained from the cubic function in the low energy region, where no data points exist to determine which line is correct, even though those sets of fitted values of the effective range parameters evenly reproduce the phase shift data accurately. Thus, we introduced the aforementioned conditions into the effective range parameters. This made the value of the ANC of the 2_1^+ state larger and caused the line of the inverse of the dressed ^{16}O propagator for $l=2$ to simply decrease. Because no verification of the conditions has been reported, we analyzed their reliability by studying the effects of the conditions on the observable of the resonant 2_4^+ state of ^{16}O and the estimate of the S_{E2} factor of $^{12}\text{C}(\alpha, \gamma)^{16}\text{O}$ at E_G .

In this study, we first investigated the elastic α - ^{12}C scattering at low energies including the resonant 2_4^+ state of ^{16}O in the cluster EFT. A set of the experimental data of the phase shift up to $E_\alpha = 10$ MeV, reported by Bruno *et al.* (1975) [30], was employed along with the precise phase shift data reported by Tischhauser *et al.* (2009) [25]. The resonant 2_4^+ state of ^{16}O appears at $E_\alpha = 4/3 E_{R(24)} = 7.9$ MeV, where $E_{R(24)}$ is the resonant energy of the 2_4^+ state of ^{16}O , $E_{R(24)} = 5.86$ MeV [5]. We introduced the conditions to restrict the parameter space of the effective range parameters in the low-energy region, $E_\alpha = 0 - 2.6$ MeV, and parameters of the S matrix of the elastic α - ^{12}C scattering for $l=2$ were fitted to the two sets of the phase shift data for three cases: one without applying the conditions to the effective range parameters and the other two applying the conditions in the parameter fit. For one of these two latter cases, we employed a value of the ANC of the 2_1^+ state of ^{16}O to fix a value of one of the effective range parameters. For all cases, the fitted parameters reproduced the phase shift data well. However, we found a large difference in the values of the ANC of the 2_1^+ state of ^{16}O ; this confirmed that the ANC of the 2_1^+ state of ^{16}O cannot be determined by the phase shift data of the elastic α - ^{12}C scattering for $l=2$. We also found noticeable differences in the values of parameters for the resonant 2_4^+ state of ^{16}O . We compared the fitted values of the resonant energy and width of the 2_4^+ state of ^{16}O with those reported in literature.

We also employed experimental data of the S_{E2} factor of $^{12}\text{C}(\alpha, \gamma)^{16}\text{O}$. First, we studied the energy dependence of the inverse of the dressed ^{16}O propagator for $l=2$ in the low-energy region. We fixed one of the effective range parameters for the large value of the ANC to reproduce a

value of the ANC of the 2_1^+ state of ^{16}O deduced from the α -transfer reactions. Then, using the fitted values of the effective range parameters for two of the three aforementioned cases, two additional parameters, $y^{(0)}$ and $h_R^{(2)}$, of $E2$ transition amplitudes of $^{12}\text{C}(\alpha, \gamma)^{16}\text{O}$ were fitted to the experimental data of the S_{E2} factor. We found the χ^2 values to be $\chi^2/N = 1.18$ and 1.55 for the cases with and without applying the conditions, respectively, where N is the number of data points of the S_{E2} factor. The S_{E2} factor was extrapolated to be $E_G = 0.3$ MeV; we found notably different values of the S_{E2} factor at E_G . We analyzed the significance of introducing the conditions in the observables of the 2_4^+ state of ^{16}O and the estimate of the S_{E2} factor at E_G , concluding that it is necessary to adopt the value of the ANC of the 2_1^+ state of ^{16}O deduced from the α -transfer reactions to reduce the uncertainty in fixing the effective range parameters of the 2_1^+ state of ^{16}O ¹⁾.

This paper is organized as follows. In Section II, we review the expression of the S matrix of the elastic α - ^{12}C scattering for $l=2$ in the cluster EFT. In Section III, the numerical results of this study are presented; in Section III.A, the conditions applied to the effective range parameters are discussed; in Section III.B, the fitting of the parameters of the S matrix for $l=2$ to the experimental phase shift data is presented, and the fitted values of the resonant energy and width of the 2_4^+ state of ^{16}O are compared with those reported in literature. In Section III.C, the energy dependence of the inverse of the dressed ^{16}O propagator for $l=2$ on the conditions in the low energy region is studied. Then, the fitting of two additional parameters of the $E2$ transition amplitudes of $^{12}\text{C}(\alpha, \gamma)^{16}\text{O}$ to the experimental data of the S_{E2} factor is presented, and we describe how the S_{E2} factor is extrapolated to E_G . The numerical results for the S_{E2} factor are presented and discussed. Finally, in Section IV, more results of this study are presented and discussed. In Appendix A, the expansion formulas of the digamma function and the inverse of the dressed ^{16}O propagator for $l=2$ are summarized; in Appendix B, the expression and derivation of the $E2$ transition amplitudes of $^{12}\text{C}(\alpha, \gamma)^{16}\text{O}$ in the cluster EFT are briefly discussed.

II. S MATRIX OF ELASTIC α - ^{12}C SCATTERING AT LOW ENERGIES

In this section, we review the expression of the S matrices of the elastic α - ^{12}C scattering at low energies and its brief derivation in the cluster EFT [23]. The S matrices of the elastic α - ^{12}C scattering for l th partial wave states are expressed in terms of phase shifts, δ_l , and elastic scattering amplitudes, \tilde{A}_l , as

$$S_l = e^{2i\delta_l} = 1 + 2ip\tilde{A}_l. \quad (1)$$

Let us assume that the phase shifts can be decomposed as

$$\delta_l = \delta_l^{(bs)} + \delta_l^{(rs1)} + \delta_l^{(rs2)} + \delta_l^{(rs3)}, \quad (2)$$

where $\delta_l^{(bs)}$ is a phase shift generated from a bound state, and $\delta_l^{(rsN)}$, with $N = 1, 2, 3$, are phase shifts generated from the first, second, and third resonant states and may have a relation with a corresponding scattering amplitude as

$$e^{2i\delta_l^{(ch)}} = 1 + 2ip\tilde{A}_l^{(ch)}, \quad (3)$$

where $ch(annel) = bs, rsN$, and $\tilde{A}_l^{(bs)}$ and $\tilde{A}_l^{(rsN)}$, with $N = 1, 2, 3$, are the amplitudes for the binding part and the first, second, and third resonant parts of the amplitudes, derived from the effective Lagrangian in Ref. [23]. The total amplitudes \tilde{A}_l for the nuclear reaction part in terms of the four amplitudes, $\tilde{A}_l^{(bs)}$ and $\tilde{A}_l^{(rsN)}$, with $N = 1, 2, 3$, read

$$\begin{aligned} \tilde{A}_l = & \tilde{A}_l^{(bs)} + e^{2i\delta_l^{(bs)}} \tilde{A}_l^{(rs1)} + e^{2i(\delta_l^{(bs)} + \delta_l^{(rs1)})} \tilde{A}_l^{(rs2)} \\ & + e^{2i(\delta_l^{(bs)} + \delta_l^{(rs1)} + \delta_l^{(rs2)})} \tilde{A}_l^{(rs3)}. \end{aligned} \quad (4)$$

Note that the total amplitudes are not obtained as the summation of amplitudes; the additional phase factors appear in front of them.

The amplitudes were calculated using the diagrams shown in Figs. 1 and 2 [19, 20, 22]. In the present study, for the elastic α - ^{12}C scattering for $l=2$, we included the subthreshold bound 2_1^+ state and three resonant 2_2^+ , 2_3^+ , 2_4^+ states of ^{16}O . For the bound state amplitude, that is, $\tilde{A}_l^{(bs)}$ with $l=2$, one has

$$\tilde{A}_2^{(bs)} = \frac{C_\eta^2 W_2(p)}{K_2(p) - 2\kappa H_2(p)}, \quad (5)$$

where $C_\eta^2 W_2(p)$ in the numerator is calculated from the initial and final state Coulomb interactions for $l=2$ in Fig. 2; p is the magnitude of relative momentum of the α - ^{12}C system in the center of mass frame, $p = \sqrt{2\mu E}$, where E is the energy of the α - ^{12}C system, and

$$W_2(p) = \frac{1}{4} (\kappa^2 + 4p^2) (\kappa^2 + p^2), \quad C_\eta^2 = \frac{2\pi\eta}{\exp(2\pi\eta) - 1}, \quad (6)$$

where η is the Sommerfeld parameter, $\eta = \kappa/p$, with κ be-

¹⁾ Recently, the ambiguity of the ANCs of all bound states of ^{16}O in the estimate of the S factors of $^{12}\text{C}(\alpha, \gamma)^{16}\text{O}$ at E_G are studied in the framework of the R -matrix analysis by Mukhamedzhanov *et al.* [31].

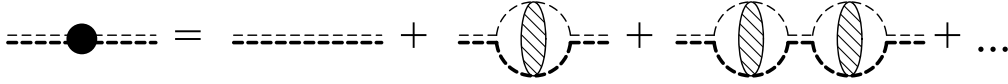


Fig. 1. Diagrams for dressed ^{16}O propagators. Thick and thin double dashed lines with or without a filled circle represent the dressed or bare ^{16}O propagators, respectively. A thick (thin) dashed line represents a propagator of ^{12}C (α), and a shaded blob in the loop diagrams represents the Coulomb Green's function.

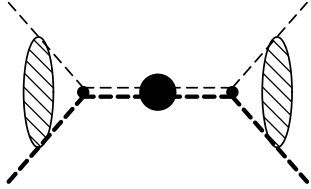


Fig. 2. Diagram for elastic α - ^{12}C scattering amplitudes. A shaded blob represents the initial or final Coulomb wave function, and a thick and thin double-dashed line with a filled circle represents a dressed ^{16}O propagator. Refer also to the caption of Fig. 1.

ing the inverse of the Bohr radius, $\kappa = Z_\alpha Z_{^{12}\text{C}} \alpha_E \mu$, where Z_A is the number of protons in a nucleus, and α_E is the fine structure constant. One has $\kappa = 245$ MeV, which is regarded as a large scale of the theory given that $\kappa > \Lambda_H$. The function $-2\kappa H_2(p)$ in the denominator of the amplitude is the Coulomb self-energy term, which is calculated from the loop diagram in Fig. 1, and one has

$$H_2(p) = W_2(p)H(\eta), \quad H(\eta) = \psi(i\eta) + \frac{1}{2i\eta} - \ln(i\eta), \quad (7)$$

where $\psi(z)$ is the digamma function. As discussed in Ref. [20], large and significant contributions to the series of effective range expansions, compared to the terms calculated using a phase shift datum at the lowest energy of the data, $E_\alpha = 2.6$ MeV [25], appear from the Coulomb self-energy term, $-2\kappa H_l(p)$, with $l=0,1,2$. In addition, for $l=2$, the large terms appear by expanding the self-energy term, $2\kappa H_2(p)$, in terms of $1/\eta^2 = (p/\kappa)^2$ at the $p \rightarrow 0$ limit. Expressions of the function $H_2(p)$ expanded in powers of $(p/\kappa)^2$ are presented in Appendix A. Thus, one has

$$2\kappa \text{Re}H_2(p) = \frac{1}{24}\kappa^3 p^2 + \frac{17}{80}\kappa p^4 + \frac{757}{4032\kappa}p^6 + \frac{289}{10080\kappa^3}p^8 + \frac{491}{22176\kappa^5}p^{10} + \dots, \quad (8)$$

where large terms proportional to κ^3 and κ appear in the first and second terms on the right-hand side of the equation. These terms do not obey the counting rules and need to be subtracted by the counter terms [32, 33].

Nuclear interaction is represented in terms of the effective range parameters in the function $K_2(p)$ in the denominator of the amplitude in Eq. (5). We introduced two

terms proportional to p^2 and p^4 as leading order contributions to subtract the two large contributions from the self-energy term mentioned above, and a term proportional to p^6 as a sub-leading one. The effective range terms up to p^6 order are included for $l=2$, and we have

$$K_2(p) = -\frac{1}{a_2} + \frac{1}{2}r_2 p^2 - \frac{1}{4}P_2 p^4 + Q_2 p^6, \quad (9)$$

where a_2 , r_2 , P_2 , and Q_2 are the effective range parameters for $l=2$.

We fixed a parameter among the four effective range parameters, a_2 , r_2 , P_2 , and Q_2 , using the condition that the inverse of the scattering amplitude $\tilde{A}_2^{(bs)}$ vanishes at the binding energy of the 2_1^+ state of ^{16}O . Thus, the denominator of the scattering amplitude,

$$D_2(p) = K_2(p) - 2\kappa H_2(p), \quad (10)$$

vanishes at $p = i\gamma_2$, where γ_2 denotes the binding momentum of the 2_1^+ state of ^{16}O ; $\gamma_2 = \sqrt{2\mu B_2} = 37.0$ MeV. Fixing the scattering length a_2 using this condition allows rewriting the expression of the function $K_2(p)$ as

$$K_2(p) = \frac{1}{2}r_2(\gamma_2^2 + p^2) + \frac{1}{4}P_2(\gamma_2^4 - p^4) + Q_2(\gamma_2^6 + p^6) + 2\kappa H_2(i\gamma_2). \quad (11)$$

At the binding energy, the wave function normalization factor $\sqrt{Z_2}$ for the bound 2_1^+ state of ^{16}O in the dressed ^{16}O propagator for $l=2$ can be expressed as

$$\frac{1}{D_2(p)} = \frac{Z_2}{E + B_2} + \dots, \quad (12)$$

where the dots denote the finite terms at $E = -B_2$, and one has

$$\sqrt{Z_2} = \left(\left| \frac{dD_2(p)}{dE} \right|_{E=-B_2} \right)^{-1/2} = \left(2\mu \left| \frac{dD_2(p)}{dp^2} \right|_{p^2=-\gamma_2^2} \right)^{-1/2}. \quad (13)$$

The wave function normalization factor $\sqrt{Z_2}$ is multiplied by a reaction amplitude when the bound state appears in the initial or final state of a reaction.

The ANCs $|C_b|_l$ for the bound states of ^{16}O are calculated using the formula of Iwinski, Rosenberg, and Spruch [34],

$$|C_b|_l = \frac{\gamma_l'}{l!} \Gamma(l+1 + \kappa/\gamma_l) \left(\left| \frac{dD_l(p)}{dp^2} \right|_{p^2 = -\gamma_l'^2} \right)^{-1/2}, \quad (14)$$

where $\Gamma(x)$ is the gamma function. Comparing Eqs. (13) and (14), it can be observed that the ANCs are proportional to the wave function normalization factor $\sqrt{Z_l}$. The ANC of the 2_1^+ state of ^{16}O , $|C_b|_2$, can be calculated by using the fitted values of the effective range parameters, r_2 , P_2 , and Q_2 .

The amplitudes for the resonant 2_2^+ , 2_3^+ , 2_4^+ states may be obtained in the Breit-Wigner-like expression as

$$\tilde{A}_2^{(rsN)} = -\frac{1}{P} \frac{\frac{1}{2}\Gamma_{(2i)}(E)}{E - E_{R(2i)} + R_{(2i)}(E) + i\frac{1}{2}\Gamma_{(2i)}(E)}, \quad (15)$$

with

$$\Gamma_{(2i)}(E) = \Gamma_{R(2i)} \frac{p C_\eta^2 W_2(p)}{p_r C_{\eta_r}^2 W_2(p_r)}, \quad (16)$$

$$R_{(2i)}(E) = a_{(2i)}(E - E_{R(2i)})^2 + b_{(2i)}(E - E_{R(2i)})^3, \quad (17)$$

where $E_{R(2i)}$ and $\Gamma_{R(2i)}$ are the energy and width of the resonant 2_i^+ states (where $i = N+1$ with $N = 1, 2, 3$), and p_r and $\eta_r = \kappa/p_r$ are the momenta and Sommerfeld factors at the resonant energies; we suppressed the i indices for them. The functions $R_{(2i)}(E)$ have the second and third order corrections expanded around $E = E_{R(2i)}$, where the coefficients $a_{(2i)}$ and $b_{(2i)}$ are fitted to the shapes of resonant peaks.

Using the relations for the amplitudes in Eqs. (5) and (15), the S matrix for $l = 2$ in Eq. (1) can be rewritten as a simple and transparent expression,

$$e^{2i\delta_2} = \frac{K_2(p) - 2\kappa \text{Re}H_2(p) + ipC_\eta^2 W_2(p)}{K_2(p) - 2\kappa \text{Re}H_2(p) - ipC_\eta^2 W_2(p)} \times \prod_{i=2}^4 \frac{E - E_{R(2i)} + R_{(2i)}(E) - i\frac{1}{2}\Gamma_{(2i)}(E)}{E - E_{R(2i)} + R_{(2i)}(E) + i\frac{1}{2}\Gamma_{(2i)}(E)}, \quad (18)$$

where we represented the part of the subthreshold state as a function of momentum, p , and the parts of the resonant states as functions of energy, E ; they are related by the non-relativistic equation $E = p^2/(2\mu)$.

III. NUMERICAL RESULTS

In this section, we first introduce the conditions to apply to the effective range parameters when fitting them to the phase shift data. We then consider two types of experimental data, namely the phase shift of the elastic α - ^{12}C scattering for $l = 2$ up to $E_\alpha = 10$ MeV and the S_{E2} factor of $^{12}\text{C}(\alpha, \gamma)^{16}\text{O}$ up to $E = 2.5$ MeV. Employing the phase shift data, we fitted the parameters of the S matrix of the elastic α - ^{12}C scattering for $l = 2$ with and without applying the conditions, and compared the fitted values of resonant energy and width of the 2_4^+ state of ^{16}O with those in literature. We also studied the energy dependence of the inverse of the dressed ^{16}O propagator for $l = 2$ in the low-energy region by using the fitted values of the effective range parameters. Then, employing the experimental data of the S_{E2} factor, we fitted additional parameters of the $E2$ transition amplitudes of $^{12}\text{C}(\alpha, \gamma)^{16}\text{O}$, and the S_{E2} factor was extrapolated to E_G .

A. Conditions applied to the effective range parameters

The inverse of the propagator, $D_2(p)$, is approximately represented as a cubic equation in powers of p^2 , whose coefficients are given by the effective range parameters r_2 , P_2 , and Q_2 . In general, it can have a minimum point and a maximum point or a flat plateau; else, it can simply decrease in the low-energy region, as mentioned above. To make it a simple decreasing function, which results in a large value of the ANC of the 2_1^+ state of ^{16}O , we introduced the conditions when fitting the effective range parameters, r_2 , P_2 , and Q_2 , in the low energy region, $0 \leq E_\alpha \leq 2.6$ MeV.

We first expanded the function $H(\eta)$ in terms of $1/\eta$ in the asymptotic limit, $\eta \rightarrow \infty$; the formulas for the expansion of the digamma function $\psi(z)$ are summarized in Appendix A. Thus, the real part of the inverse of the propagator, $\text{Re}D_2(p)$, in Eq. (10) becomes expanded around the binding energy, $E = -B_2$, i.e., $p^2 = -\gamma_2'^2$, yielding

$$\text{Re}D_2(p) \simeq \sum_{n=1}^5 C_n (\gamma_2'^2 + p^2)^n, \quad (19)$$

with

$$C_1 = \frac{1}{2} \left(r_2 - \frac{1}{12} \kappa^3 \right) + \frac{1}{2} \left(P_2 + \frac{17}{20} \kappa \right) \gamma_2'^2 + 3 \left(Q_2 - \frac{757}{4032 \kappa} \right) \gamma_2'^4 + \frac{289}{2520 \kappa^3} \gamma_2'^6 - \frac{2455}{22176 \kappa^5} \gamma_2'^8 + \dots, \quad (20)$$

$$C_2 = -\frac{1}{4} \left(P_2 + \frac{17}{20} \kappa \right) - 3 \left(Q_2 - \frac{757}{4032\kappa} \right) \gamma_2^2 - \frac{289}{1680\kappa^3} \gamma_2^4 + \frac{2455}{11088\kappa^5} \gamma_2^6 - \dots, \quad (21)$$

$$C_3 = Q_2 - \frac{757}{4032\kappa} + \frac{289}{2520\kappa^3} \gamma_2^2 - \frac{2455}{11088\kappa^5} \gamma_2^4 + \dots, \quad (22)$$

$$C_4 = -\frac{289}{10080\kappa^3} + \frac{2455}{22176\kappa^5} \gamma_2^2 - \dots, \quad (23)$$

$$C_5 = -\frac{491}{22176\kappa^5} + \dots, \quad (24)$$

and the conditions $C_n < 0$ for $n = 1, 2, 3$ are introduced, which make $\text{Re}D_2(p)$ simply decrease in the low energy region (one may notice that $C_4, C_5 < 0$ above). These conditions lead to restrictions on the effective range parameters,

$$Q_2 < \frac{757}{4032\kappa} - \frac{289}{2520\kappa^3} \gamma_2^2 + \frac{2455}{11088\kappa^5} \gamma_2^4 + \dots, \quad (25)$$

$$P_2 > -\frac{17}{20} \kappa - 12 \left(Q_2 - \frac{757}{4032\kappa} \right) \gamma_2^2 - \frac{289}{420\kappa^3} \gamma_2^4 + \frac{2455}{2772\kappa^5} \gamma_2^6 + \dots, \quad (26)$$

$$r_2 < \frac{1}{12} \kappa^3 - \left(P_2 + \frac{17}{20} \kappa \right) \gamma_2^2 - 6 \left(Q_2 - \frac{757}{4032\kappa} \right) \gamma_2^4 - \frac{289}{1260\kappa^3} \gamma_2^6 + \frac{2455}{11088\kappa^5} \gamma_2^8 + \dots, \quad (27)$$

where the terms are expanded in powers of $(\gamma_2/\kappa)^2 = 0.023$ [$< (Q/\Lambda_H)^2 = 0.0625$]; the truncation of higher-order terms would be a good approximation. From those conditions, the minimum or maximum values of the effective range parameters are

$$\begin{aligned} r_{2,\max} &= 0.159026 \text{ fm}^{-3}, \\ P_{2,\min} &= -1.05390 \text{ fm}^{-1}, \\ Q_{2,\max} &= 0.149343 \text{ fm}. \end{aligned} \quad (28)$$

Note that the wave function normalization factor Z_2 in Eq. (13) is obtained from C_1 in Eq. (20) as $Z_2^{-1} = -2\mu C_1$ (note that C_1 is negative), and the ANC of the 2_1^+ state of ^{16}O is expressed as

$$|C_b|_2 = \frac{1}{2} \gamma_2^2 \Gamma(3 + \kappa/\gamma_2) \frac{1}{\sqrt{-C_1}}. \quad (29)$$

Thus, if one adopts the ANC of the 2_1^+ state of ^{16}O , $|C_b|_2$, as an input, one of the three effective range parameters, r_2 , P_2 , and Q_2 , in C_1 can be fixed by this equation.

B. Fitting the effective range parameters and the 2_4^+ state of ^{16}O

In a previous study of ours [22], we employed precise phase shift data up to $E_\alpha = 6.62$ MeV reported by Tischhauser *et al.* (2009) [25] to fit the parameters, including the resonant 2_2^+ and 2_3^+ states of ^{16}O . (They appear at $E_\alpha(2_2^+) = 3.58$ MeV and $E_\alpha(2_3^+) = 5.81$ MeV.) We obtained six sets of values for the effective range parameters, r_2 , P_2 , and Q_2 , which fitted the precise phase shift data for $l = 2$ well (see Tables 1 and 2 in Ref. [23]). However, these values yielded different values of the ANC of the 2_1^+ state of ^{16}O and different paths of the real part of the inverse of the dressed ^{16}O propagator for $l = 2$, $\text{Re}D_2(p)$, in the low energy region where the S_{E2} factor was extrapolated to E_G (see Fig. 6 in Ref. [23]). In the present study, we employed and included a set of phase shift data for $l = 2$ up to $E_\alpha = 10$ MeV reported by Bruno *et al.* (1975) [30] to refit the parameters, explicitly including the resonant 2_4^+ state of ^{16}O in the S matrix of the elastic α - ^{12}C scattering for $l = 2$. There are 13 parameters (12 parameters when r_1 is fixed by $|C_b|_2$), $\theta = \{r_2, P_2, Q_2, E_{R(22)}, \Gamma_{R(22)}, E_{R(23)}, \Gamma_{R(23)}, a_{(23)}, b_{(23)}, E_{R(24)}, \Gamma_{R(24)}, a_{(24)}, b_{(24)}\}$, which were fitted to the two sets of phase shift data; we introduced the conditions to the effective range parameters by means of the χ^2 fit using an MCMC ensemble sampler [35].

Table 1 presents values of the parameters fitted to the phase shift data. The second column lists values from a previous study of ours (column (I) in Table 2) [22]. The third column lists values obtained in the present study without applying the conditions. The fourth and fifth columns list values obtained in this study by applying the conditions in Eqs. (25), (26), and (27) to the effective range parameters. The fifth column lists the values of the ANC of the 2_1^+ state of ^{16}O , $|C_b|_2 = 10 \times 10^4 \text{ fm}^{-1/2}$, adopted to fix one of the effective range parameters, r_2 . In the aforementioned previous study, we employed experimental data reported by Tischhauser *et al.* (2009) [25] (number of data points: $N = 245$); we included the 2_4^+ state as a background from high energy, where the resonant energy and width were fixed by using experimental data [5], and the parameters $a_{(24)}$ and $b_{(24)}$ were not included. One can see that the values in the second and third columns are in good agreement except for those of $\Gamma_{R(24)}$ and χ^2/N . We discuss the values of $\Gamma_{R(24)}$ later on. The larger values of χ^2/N are due to the inclusion of the phase shift data reported by Bruno *et al.* (1975) [30]

Table 1. Fitted values of the parameters of the S matrix of the elastic α - ^{12}C scattering for $l = 2$ to the two sets of phase shift data [25, 30]. The second column lists values from column (I) in Table 2 from a previous study of ours [22]; the third column lists values obtained in this study without applying the conditions; the fourth and fifth columns list values obtained in this study applying the conditions to the effective range parameters in Eqs. (25), (26), and (27); and the fifth column lists the values of the ANC of the 2_1^+ state of ^{16}O , $|C_b|_2 = 10 \times 10^4 \text{ fm}^{-1/2}$, employed to fix the corresponding values of r_2 (marked by *). The second row from the bottom includes values of the ANC of the 2_1^+ state of ^{16}O calculated using the values of r_2 , P_2 , and Q_2 . The last row presents values of χ^2/N (where N is the number of data). In the aforementioned previous study, $E_{R(24)}$ and $\Gamma_{R(24)}$ were included as fixed values (marked by *) using the experimental data [5]; the parameters $a_{(24)}$ and $b_{(24)}$ were not included.

	Prev. work w/o cond.	This work w/o cond.	This work w cond.(1)	This work w cond.(2)
r_2/fm^{-3}	0.149(4)	0.150(6)	0.1586(3)	0.1575*
P_2/fm^{-1}	-1.19(5)	-1.18(8)	-1.047(2)	-1.049(2)
Q_2/fm	0.081(16)	0.084(3)	0.138(2)	0.141(2)
$E_{R(22)}/\text{MeV}$	2.68308(5)	2.68308(1)	2.68308(1)	2.68308(1)
$\Gamma_{R(22)}/\text{keV}$	0.75(2)	0.76(1)	0.76(1)	0.76(1)
$E_{R(23)}/\text{MeV}$	4.3545(2)	4.3533(3)	4.3537(1)	4.3536(1)
$\Gamma_{R(23)}/\text{keV}$	74.61(3)	74.5(1)	74.5(1)	74.5(1)
$a_{(23)}/\text{MeV}^{-1}$	0.46(12)	0.6(2)	1.1(1)	1.2(1)
$b_{(23)}/\text{MeV}^{-2}$	0.47(9)	0.5(2)	0.6(1)	0.6(1)
$E_{R(24)}/\text{MeV}$	5.858*	5.92(2)	5.90(2)	5.89(2)
$\Gamma_{R(24)}/\text{keV}$	150*	300^{+60}_{-40}	235(20)	237(19)
$a_{(24)}/\text{MeV}^{-1}$	—	0.3(4)	0.6(1)	0.67(9)
$b_{(24)}/\text{MeV}^{-2}$	—	$0.96^{+0.79}_{-0.50}$	0.3(1)	0.2(1)
$ C_b _2/\text{fm}^{-1/2}$	$3.1(6) \times 10^4$	3.24×10^4	22.8×10^4	10×10^4 *
χ^2/N (N)	0.66 (245)	3.02 (271)	3.04 (271)	3.05 (271)

Table 2. Resonant energy and width of the 2_4^+ state of ^{16}O . The values in the second, third, and fourth columns are extracted from literature: Bruno *et al.* (1975) [30], the compilation edited by Tilley, Weller, and Cheves (TWC) (1993) [5], and deBoer *et al.* (2012) [36], respectively. Those in the fifth and sixth columns are the fitted values obtained in this study without and with the conditions applied to the effective range parameters.

	Bruno (1975)	TWC (1993)	deBoer (2012)	This work w/o cond.	This work w cond.(1)
$E_{R(24)}/\text{MeV}$	5.83(3)	5.858(10)	5.805(2)	5.92(2)	5.90(2)
$\Gamma_{R(24)}/\text{keV}$	520(200)	150(10)	349(3)	300^{+60}_{-40}	235(20)

(number of data points: $N = 26$). We found that the conditions applied to the effective range parameters change the values of r_2 , P_2 , and Q_2 significantly, as shown in the third to fifth columns. Note that the values of the effective range parameters in the second and third columns do not satisfy the bounds owing to the conditions in Eq. (28), whereas those in the fourth and fifth columns do satisfy them. The values of ANC, $|C_b|_2$, are altered largely; we obtained $|C_b|_2 = 3.24 \times 10^4 \text{ fm}^{-1/2}$ when the conditions were not applied, which is larger by approximately a factor of 1.6 than the value reported by König, Lee, and Hammer. This may be due to the inclusion of the 2_4^+ state of ^{16}O (see Ref. [22]). We obtained $|C_b|_2 = 22.8 \times 10^4 \text{ fm}^{-1/2}$ when applying the conditions in the fourth column, which is larger by approximately a factor of 2 than the values deduced from the α -transfer reactions. This range

of values of the ANC, $|C_b|_2 = (3.2 - 22.8) \times 10^4 \text{ fm}^{-1/2}$, agrees with that reported by Sparenberg, Capel, and Baye in their study employing a potential model, $(2 - 18) \times 10^4 \text{ fm}^{-1/2}$ [28]. In addition, the values of χ^2/N in the third to fifth columns are similar. We confirmed that the ANC of the 2_1^+ state of ^{16}O cannot be determined by the phase shift data of the elastic α - ^{12}C scattering for $l = 2$. Note also that the values of the shape parameter, $a_{(23)}$, of the 2_3^+ state and the width and shape parameters, $\Gamma_{R(24)}$, $a_{(24)}$, and $b_{(24)}$, of the 2_4^+ state are altered between the third column and the fourth and fifth columns in Table 1.

In Fig. 3, the phase shifts of the elastic α - ^{12}C scattering for $l = 2$ are represented as functions of the α energy E_α . The solid line represents the values of the parameters in the third column in Table 1. The dotted line represents the values in the fourth column of the same table. The ex-

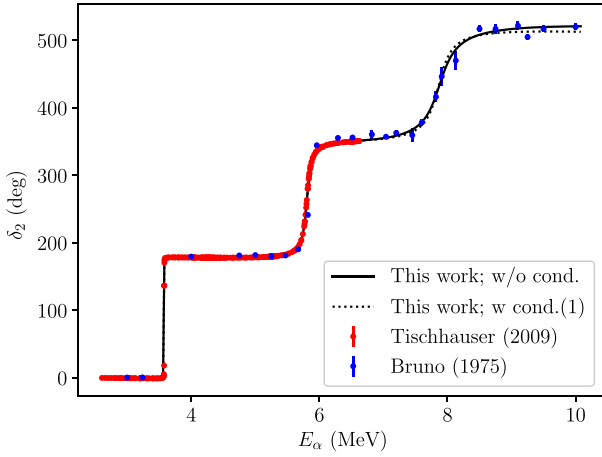


Fig. 3. (color online) Phase shifts of the elastic α - ^{12}C scattering for $l=2$ represented as functions of the α energy E_α in the laboratory frame. The solid line represents the values of the parameters in the third column in Table 1, whereas the dotted line represents the values in the fourth column in the same table. The experimental data reported by Tischhauser *et al.* (2009) [25] and Bruno *et al.* (1975) [30] are represented in the figure as well.

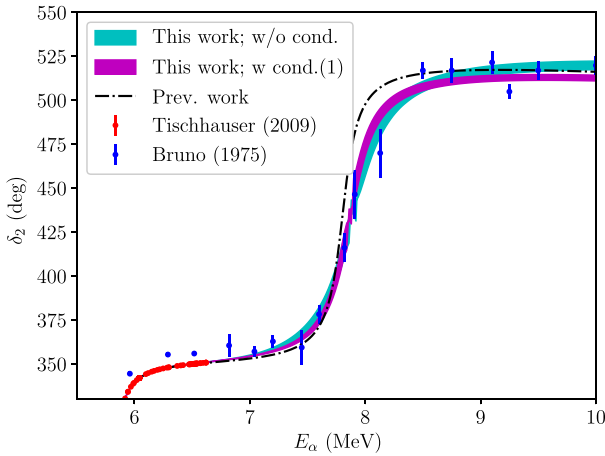


Fig. 4. (color online) Same phase shifts with the bands represented in Fig. 3 in the energy region of the resonant 2_4^+ state, represented as functions of the α energy E_α . The bands, spanning 16% to 84% distribution of a phase shift, are calculated from the samples of the parameters in the MCMC analysis. The dashed-dotted line represents the parameters obtained in the previous study (those in the second column in Table 1). Refer also to the caption of Fig. 3.

perimental data reported by Tischhauser *et al.* (2009) [25] (accurate data up to the p - ^{15}N breakup energy, $E_\alpha = 6.62$ MeV) and Bruno *et al.* (1975) [30] (data covering the high-energy region for the resonant 2_4^+ state of ^{16}O up to $E_\alpha = 10$ MeV) are also represented in the figure. Note that both lines reproduce the experimental data well.

In Fig. 4, the same lines with the bands and data shown in Fig. 3 are represented in the energy region for

the resonant 2_4^+ state of ^{16}O . The dashed-dotted line represents the parameters obtained in the previous study (those in the second column in Table 1). The bands represent the uncertainty of the phase shifts, which are calculated as the band from 16% to 84% distribution of a phase shift calculated from the samples of the parameters in the MCMC analysis. Note that the bands fitted to the data in this study are more accurate than those in the previous study. The two bands in this study are distinguishable. However, the data exhibit large error bars; it is not easy to determine which line is more accurate. As discussed above, this difference is also observed in the different values of the parameters of the 2_4^+ state of ^{16}O in the third and fourth columns of Table 1.

In Table 2, we summarize the values of the resonant energy and width of the 2_4^+ state of ^{16}O , $E_{R(24)}$ and $\Gamma_{R(24)}$, reported in literature and our results presented in Table 1. We obtained larger values of the resonant energy, $E_{R(24)}$, by two sigma deviation with respect to the value of Bruno *et al.* (1975) [30]. Note that the values of $\Gamma_{R(24)}$ reported in literature are still scattered, and their uncertainties are significant; these values are in good agreement within the error bars, except for the compilation edited by Tilley, Weller, and Cheves (1993) [5], with $\Gamma_{R(24)} = 150(10)$ keV, which is significantly smaller than the others. To improve this situation, it may be helpful to have a more precise data set of the phase shift in the energy region for the resonant 2_4^+ state of ^{16}O . Note that because two channels, α - $^{12}\text{C}^*(2_1^+)$ and p - ^{15}N states, open in this energy region, the inelastic channels of the scattering start contributing. Thus, it is necessary to improve the theoretical framework as well.

C. Dressed ^{16}O propagator and estimate of the S_{E2} factor at E_G

We can now study the effect of the conditions applied to the effective range parameters on the inverse of the propagator, $D_2(p)$, and on the calculation of the S_{E2} factor of the $E2$ transition of $^{12}\text{C}(\alpha, \gamma)^{16}\text{O}$. In Fig. 5, we represent the real part of $D_2(E)$ [$= D_2(p)$] as a function of the energy E of the α - ^{12}C system in the center-of-mass frame of the low-energy region. The solid line was obtained using the values of r_2 , P_2 , and Q_2 in the third column of Table 1, whereas the dotted line was obtained using the values in the fourth column of the same table. The experimental data of the phase shift reported by Tischhauser *et al.* (2009) [25] were converted to $\text{Re}D_2(E)$ through the relation

$$\text{Re}D_2(p) = pW_2(p)C_\eta^2 \cot \delta_2, \quad (30)$$

and represented in the figure as well. Note that the paths of both lines are notably different because of the conditions applied (or not applied) to the effective range para-

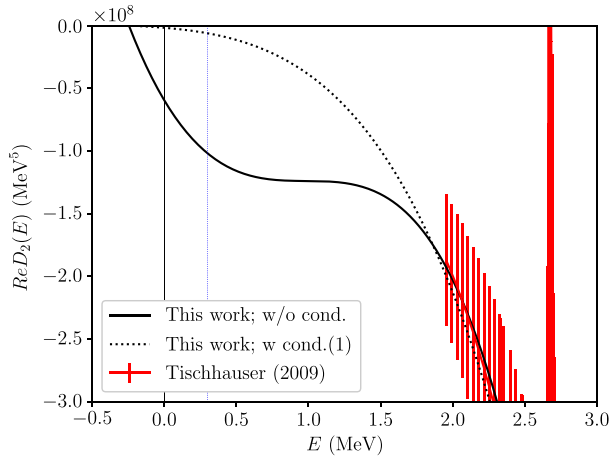


Fig. 5. (color online) Real part of the inverse of the propagator, $\text{Re}D_2(E)$ [$=\text{Re}D_2(p)$], represented as a function of the energy E of the α - ^{12}C system in the center-of-mass frame. The solid line is represented using the values of the effective range parameters, r_2 , P_2 , and Q_2 , in the third column in Table 1, whereas the dotted line is represented using the values in the fourth column in the same table. The phase shift data reported by Tischhauser *et al.* (2009) [25] are converted and represented in the figure as well. A vertical blue line is drawn at $E_G = 0.3$ MeV.

eters. The solid line exhibits a plateau in the low energy region, $0 < E < 1.95$ MeV, whereas the dotted line decreases smoothly. Both lines reproduce the experimental data equally well. In addition, at the top of the figure, both lines start at the same point, *i.e.*, at the binding energy of the 2_1^+ state of ^{16}O , $E = -B_2$, where $D_2(-B_2) = 0$. Note also that the gradients of the lines at this point are also notably different; they are related to the values of the ANC of the 2_1^+ state of ^{16}O , $|C_b|_2$, in Eq. (14). Because the square of the root of the gradient appears in the denominator of the formula of $|C_b|_2$, a large negative angle associated with the horizontal line at this point leads to a small value of the ANC, whereas a small negative angle leads to a large value of the ANC. Thus, we obtained notably different values: small and large values of the ANC, as shown in Table 1. Both lines go through different paths between the point at $E = -B_2$ and the datum of phase shift

whose lowest energy is $E = 3/4E_\alpha = 1.95$ MeV. Because the inverse of the propagator $D_2(p)$ appears in the denominator of the $E2$ transition amplitudes of $^{12}\text{C}(\alpha, \gamma)^{16}\text{O}$, the energy dependence of $D_2(E)$ [$=D_2(p)$] in the low energy region is crucial when extrapolating the S_{E2} factor to $E_G = 0.3$ MeV.

By employing the two sets of fitted values of the effective range parameters in the third and fifth columns in Table 1, we fitted additional parameters in the $E2$ transition amplitudes of $^{12}\text{C}(\alpha, \gamma)^{16}\text{O}$ to the experimental data of the S_{E2} factor of $^{12}\text{C}(\alpha, \gamma)^{16}\text{O}$. The expression of the $E2$ transition amplitudes and its brief derivation are presented in Appendix B; we have two additional parameters, $h_R^{(2)}$ and $y^{(0)}$, in the amplitudes. The experimental data of the S_{E2} factor below the resonant energy of 2_2^+ of ^{16}O , up to $E = 2.5$ MeV, reported by Ouellet *et al.* (1996) [37], Roters *et al.* (1999) [38], Kunz *et al.* (2001) [39], Fey (2004) [40], Makii *et al.* (2009) [41], and Plag *et al.* (2012) [42], were employed for fitting.

In Table 3, fitted values of the parameters $h_R^{(2)}$ and $y^{(0)}$ are presented along with the χ^2/N values. When fitting these parameters, we used the values of the effective range parameters, r_2 , P_2 , and Q_2 , listed in the third and fifth columns in Table 1. Values of the S_{E2} factor at $E_G = 0.3$ MeV were calculated using the fitted values of the parameters $h_R^{(2)}$ and $y^{(0)}$ and included in the table as well. Note that the fitted values of the parameters $h_R^{(2)}$ and $y^{(0)}$ are still scattered for both cases. The χ^2/N values in the last two columns are $\chi^2/N = 1.55$ and 1.18 , and the deduced values of S_{E2} at E_G show a difference of a factor of ten. We obtained $S_{E2} = 4.1 \pm 0.2$ and 40^{+14}_{-12} keVb, respectively. These two values are still within the range of previously reported values of the S_{E2} factor summarized in Table IV in Ref. [9].

In Fig. 6, two bands of the S_{E2} factor of $^{12}\text{C}(\alpha, \gamma)^{16}\text{O}$ are represented as functions of the energy E of the initial α - ^{12}C state in the center-of-mass frame. The experimental data of the S_{E2} factor are included in the figure as well. The cyan band for the S_{E2} factor, which exhibits a minimum point and a maximum point, was calculated using the fitted values of the parameters for which the conditions set to the effective range parameters were not ap-

Table 3. Values of $h_R^{(2)}$ and $y^{(0)}$ fitted to the experimental data of the S_{E2} factor using two sets of values of the effective range parameters, r_2 , P_2 , and Q_2 . We used the values of r_2 , P_2 , Q_2 listed in the third column of Table 1 for the values in the second column. For those in the third column, we used the values of r_2 , P_2 , and Q_2 listed in the fifth column of Table 1. The χ^2/N values for fitting are included in the table as well. S_{E2} at $E_G = 0.3$ MeV was calculated using the fitted parameters.

$ C_b _2/\text{fm}^{-1/2}$	This work (w/o cond.) 3.2×10^4	This work (w cond.(2)) 10×10^4
$h_R^{(2)} \times 10^{-11}/\text{MeV}^4$	50.6 ± 0.4	$45.53^{+0.04}_{-0.03}$
$y^{(0)}/\text{MeV}^{-1/2}$	$1.99 \pm 0.01 \times 10^{-3}$	$5.9 \pm 0.1 \times 10^{-2}$
χ^2/N ($N = 51$)	1.55	1.18
S_{E2}/keVb at E_G	4.1 ± 0.2	40^{+14}_{-12}

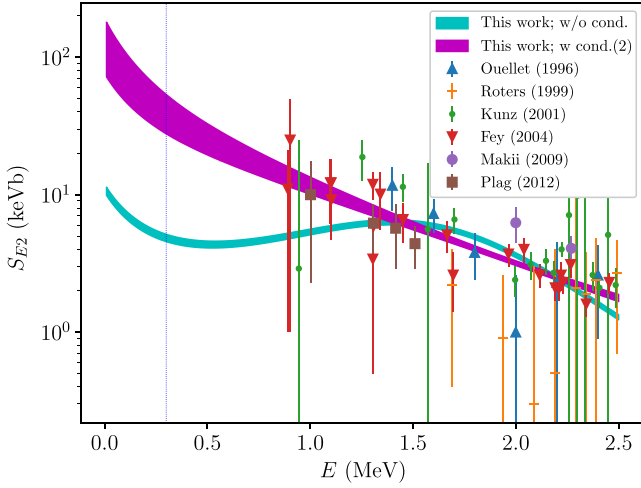


Fig. 6. (color online) S_{E2} factor of $^{12}\text{C}(\alpha, \gamma)^{16}\text{O}$ represented as a function of the energy E of the initial α - ^{12}C state in the center-of-mass frame. The two bands are plotted using the fitted parameters presented in Table 3. The bands, which correspond to the 16% to 84% distributions of the S_{E2} factor, are calculated from the samples of the parameters $h_R^{(2)}$ and $y^{(0)}$ in the MCMC analysis. The experimental data (see the text) are included in the figure as well. The vertical blue line marks $E_G = 0.3$ MeV.

plied. The magenta band of the S_{E2} factor, which decreases, was calculated using the fitted values for which the conditions were applied; one of the three effective range parameters was constrained by the value of the ANC, $|C_b|_2 = 10 \times 10^4 \text{ fm}^{-1/2}$, according to Eq. (29). Note that the energy dependence of the S_{E2} factor mainly results from that of $D_2(E)$, which appears in the denominator of the $E2$ transition amplitudes of $^{12}\text{C}(\alpha, \gamma)^{16}\text{O}$, shown in Fig. 5. The χ^2/N values of the bands are 1.55 and 1.18, respectively, which indicates that the magenta band is better to fit the data than the cyan one.

IV. RESULTS AND DISCUSSION

In this study, we first analyzed the elastic α - ^{12}C scattering for $l=2$ introducing conditions applied to the effective range parameters, r_2 , P_2 , and Q_2 , when fixing them to the phase shift data. We employed two data sets for elastic scattering: one featuring precise phase shift data up to the p - ^{15}N breakup energy, $E_\alpha = 6.62$ MeV, reported by Tischhauser *et al.* (2009) [25], and the other featuring data up to $E_\alpha = 10$ MeV, covering the resonant 2_4^+ state of ^{16}O , as reported by Bruno *et al.* (1975) [30]. We fitted the parameters of the S matrix of the elastic α - ^{12}C scattering for $l=2$ to the phase shift data for three cases: one without applying the conditions and the other two applying the conditions to the effective range parameters in the low-energy region, where no experimental data have been reported. In one of the two cases with the

conditions applied, the value of the ANC of the 2_1^+ state of ^{16}O , $|C_b|_2 = 10 \times 10^4 \text{ fm}^{-1/2}$, was used to fix one of the effective range parameters, r_2 . We found larger values of the width of the 2_4^+ state of ^{16}O , $\Gamma_{R(24)} = 235(20)$ and 300_{-40}^{+60} keV, than those listed in the compilation, $\Gamma_{R(24)} = 150(10)$ keV [5]. We also found large and small values of the ANC of the 2_1^+ state of ^{16}O , $|C_b|_2 = 23.3 \times 10^4$ and $3.24 \times 10^4 \text{ fm}^{-1/2}$, for two of the three cases. The three sets of fitted parameters reproduced the phase shift data equally well. The fitted values of the effective range parameters for two sets of the three cases were employed for the study of the S_{E2} factor of $^{12}\text{C}(\alpha, \gamma)^{16}\text{O}$. First, we studied the energy dependence of the inverse of the ^{16}O propagator for $l=2$ in the low energy region where the S_{E2} factor is extrapolated to E_G . Then, we fitted two additional parameters, $h_R^{(2)}$ and $y^{(0)}$, of the $E2$ transition amplitude of $^{12}\text{C}(\alpha, \gamma)^{16}\text{O}$ to the experimental data of the S_{E2} factor with the following two χ^2/N values: $\chi^2/N = 1.18$ and 1.55. We extrapolated the S_{E2} factor to E_G , where, as mentioned, we fixed one of the effective range parameters for the case of the large ANC by adopting the ANC of the 2_1^+ state of ^{16}O deduced from the α -transfer reactions, $|C_b|_2 = 10 \times 10^4 \text{ fm}^{-1/2}$. We obtained $S_{E2} = 40_{-12}^{+14}$ and 4.1 ± 0.2 keVb at $E_G = 0.3$ MeV, respectively. We found that both values are within the range of previously reported values of S_{E2} at E_G reported in literature.

There is no restriction on whether one should apply the conditions to the effective range parameters or not when fitting to the phase shift data because the phase shift data were equally well-fitted for all cases. In other words, for the phase shift data for $l=2$, it is not possible to determine which line drawn in Fig. 5 is better, while it is crucial to extrapolate the S_{E2} factor to E_G . One may argue that it is necessary to introduce the conditions because of the simplicity of natural laws, as once stated by Poincaré: "natural laws must be simple" [43]. For the present case, one may regard that the dotted line (which simply decreases) is simpler than the solid line (which exhibits a plateau) in Fig. 5; the appearance of such a bump in the S_{E2} factor in Fig. 6 might indicate interference with an unknown bound or resonant state at low energies. This assumption should be tested experimentally or using other possible methods.

A quantity that could test a verification of the conditions may be the width of the resonant 2_4^+ state of ^{16}O . The reported values listed in Table 2 are still scattered. Nevertheless, the value $\Gamma_{R(24)} = 349(3)$ keV recently reported by deBoer *et al.* (2012) could support the result of $\Gamma_{R(24)} = 300_{-40}^{+60}$ keV, which was obtained without applying the conditions. Meanwhile, as discussed above, we need to improve the theoretical framework because new channels start opening in this energy region.

The experimental data of the S_{E2} factor of $^{12}\text{C}(\alpha, \gamma)^{16}\text{O}$ may provide another quantity to test the verification of the conditions because the data cover a lower energy re-

gion, $E = 0.9 - 1.95$ MeV ($E_\alpha = 4/3E = 1.2 - 2.6$ MeV), than those of the elastic α - ^{12}C scattering. However, the data of the S_{E2} factor exhibit large error bars, especially in the lower energy region, $E = 0.9 - 1.2$ MeV. After fitting the parameters $h_R^{(2)}$ and $y^{(0)}$ of the $E2$ transition amplitudes of $^{12}\text{C}(\alpha, \gamma)^{16}\text{O}$, we obtained the χ^2/N values for two of the three cases: $\chi^2/N = 1.18$ and 1.55 . This may support the application of the conditions in the low-energy region although the data of the S_{E2} factor still present large uncertainties. More accurate measurements of the S_{E2} factor in the energy range $E = 0.9 - 1.5$ MeV would be helpful to obtain a clear conclusion.

The values of the ANC of the 2_1^+ state of ^{16}O obtained in this study are notably different for the cases $|C_{b|_2} = 3.24 \times 10^4$ and $23.3 \times 10^4 \text{ fm}^{-1/2}$. As previously mentioned, the values of $|C_{b|_2}$ are deduced from α -transfer reactions such as $^{12}\text{C}(^6\text{Li}, d)^{16}\text{O}$ [44]; the value of $|C_{b|_2}$ was recently updated by Hebborn *et al.* to be $|C_{b|_2} = 10.7(3) \times 10^4 \text{ fm}^{-1/2}$ [45]. They used the ANC of the ground state of ^6Li as d - α system deduced from ab initio calculations [46]. As discussed above, we employed a value of the ANC, $|C_{b|_2} = 10 \times 10^4 \text{ fm}^{-1/2}$, adopted from α -transfer reactions to constrain the values of the effective range parameters according to Eq. (29) when fitting them to the phase shift data applying the conditions. We obtained $S_{E2} = 40_{-12}^{+14} \text{ keV b}$ with $\chi^2/N = 1.18$. This χ^2 value is small but the error of the S_{E2} factor is significantly large, approximately 35%. This may also result from the large errors of the data of the S_{E2} factor. Thus, it would be important to reduce the error bar of the S_{E2} factor theoretically estimated using the other available experimental data. A study in this direction is now being conducted.

ACKNOWLEDGEMENTS

The author would like to thank D. Phillips, T. Kajino, R. deBoer, and C. H. Hyun for discussions.

APPENDIX A

In this appendix, we discuss the relations related to the function $H_2(p)$ in Eq. (7) in the low energy limit, $p \rightarrow 0$. Let us consider two formulas of the digamma function $\psi(z)$; one is Eq. 6.3.18 in Ref. [47],

$$\begin{aligned} \psi(z) &\sim \ln z - \frac{1}{2z} - \sum_{n=1}^{\infty} \frac{B_{2n}}{2nz^{2n}} \\ &= \ln z - \frac{1}{2z} - \frac{1}{12z^2} - \frac{1}{120z^4} - \frac{1}{252z^6} - \dots, \end{aligned} \quad (\text{A1})$$

for $|z| \rightarrow \infty$ and $|\arg z| < \pi$, where B_{2n} are Bernoulli numbers,

$$B_2 = \frac{1}{6}, \quad B_4 = -\frac{1}{30}, \quad B_6 = \frac{1}{42}, \quad B_8 = -\frac{1}{30}, \quad B_{10} = \frac{5}{66}, \quad \dots, \quad (\text{A2})$$

and the other is Eq. 5.4.16 in Ref. [48],

$$\text{Im}\psi(iy) = \frac{1}{2y} + \frac{\pi}{2} \coth(\pi y), \quad (\text{A3})$$

allowing us to rewrite the imaginary and real parts of the function $H(\eta)$ in Eq. (7) as

$$\text{Im}H(\eta) = \text{Im}\psi(i\eta) - \frac{1}{2\eta} - \pi = \frac{1}{2\eta} \frac{2\pi\eta}{e^{2\pi\eta} - 1} = \frac{1}{2\eta} C_\eta^2, \quad (\text{A4})$$

$$\begin{aligned} \text{Re}H(\eta) &= \text{Re}\psi(i\eta) - \ln \eta = - \sum_{n=1}^{\infty} \frac{B_{2n}}{2n(i\eta)^{2n}} = \frac{1}{12\eta^2} \\ &+ \frac{1}{120\eta^4} + \frac{1}{252\eta^6} + \frac{1}{240\eta^8} + \frac{1}{132\eta^{10}} + \dots. \end{aligned} \quad (\text{A5})$$

This allows obtaining the expression of $2\kappa \text{Re}H_2(p)$ in Eq. (8).

The expressions of $\text{Re}D_2(p)$ in Eq. (19) is calculated as follows. First, one may expand the $H(\eta)$ function using the equation above. We obtain an expression of $\text{Re}D_2(p)$,

$$\begin{aligned} \text{Re}D_2(p) &= a(\gamma_2^2 + p^2) + b(\gamma_2^4 - p^4) + c(\gamma_2^6 + p^6) + d(\gamma_2^8 - p^8) \\ &+ e(\gamma_2^{10} + p^{10}) + \dots, \end{aligned} \quad (\text{A6})$$

where a , b , c , d , and e are coefficients. Explicitly, we have

$$\begin{aligned} \text{Re}D_2(p) &= \left(\frac{1}{2}r_2 - \frac{1}{24}\kappa^3\right)(\gamma_2^2 + p^2) + \left(\frac{1}{4}P_2 + \frac{17}{80}\kappa\right)(\gamma_2^4 - p^4) \\ &+ \left(Q_2 - \frac{757}{4032\kappa}\right)(\gamma_2^6 + p^6) + \frac{289}{10080\kappa^3}(\gamma_2^8 - p^8) \\ &- \frac{491}{22176\kappa^5}(\gamma_2^{10} + p^{10}) + \dots. \end{aligned} \quad (\text{A7})$$

Then, one may use the relations

$$\gamma_2^4 - p^4 = -(\gamma_2^2 + p^2)^2 + 2\gamma_2^2(\gamma_2^2 + p^2), \quad (\text{A8})$$

$$\gamma_2^6 + p^6 = (\gamma_2^2 + p^2)^3 - 3\gamma_2^2(\gamma_2^2 + p^2)^2 + 3\gamma_2^4(\gamma_2^2 + p^2), \quad (\text{A9})$$

$$C_4 = -d - 5\gamma_2^2 e, \quad (\text{A16})$$

$$\gamma_2^8 - p^8 = -(\gamma_2^2 + p^2)^4 + 4\gamma_2^2(\gamma_2^2 + p^2)^3 - 6\gamma_2^4(\gamma_2^2 + p^2)^2 + 4\gamma_2^6(\gamma_2^2 + p^2), \quad (\text{A10})$$

$$C_5 = e. \quad (\text{A17})$$

$$\gamma_2^{10} + p^{10} = (\gamma_2^2 + p^2)^5 - 5\gamma_2^2(\gamma_2^2 + p^2)^4 + 10\gamma_2^4(\gamma_2^2 + p^2)^3 - 10\gamma_2^6(\gamma_2^2 + p^2)^2 + 5\gamma_2^8(\gamma_2^2 + p^2), \quad (\text{A11})$$

Finally, we obtain the expressions of the coefficients C_i , with $i = 1, 2, 3, 4, 5$, in Eqs. (20)–(24).

APPENDIX B

In this appendix, we present the expression of the $E2$ transition amplitudes of $^{12}\text{C}(\alpha, \gamma)^{16}\text{O}$ and briefly discuss its derivation. Figure B1 shows the diagrams of the reaction. The vertex functions and propagators are derived from the effective Lagrangian. We obtain the $E2$ transition amplitude of $^{12}\text{C}(\alpha, \gamma)^{16}\text{O}$ as

$$A^{(l=2)} = \vec{\epsilon}_{(\gamma)}^* \cdot \hat{p} \hat{k}' \cdot \hat{p} X^{(l=2)}, \quad (\text{B1})$$

obtaining

$$\text{Re}D_2(p) \approx \sum_{n=1}^5 C_n (\gamma_2^2 + p^2)^n, \quad (\text{A12})$$

with

$$C_1 = a + 2\gamma_2^2 b + 3\gamma_2^4 c + 4\gamma_2^6 d + 5\gamma_2^8 e, \quad (\text{A13})$$

$$C_2 = -b - 3\gamma_2^2 c - 6\gamma_2^4 d - 10\gamma_2^6 e, \quad (\text{A14})$$

$$C_3 = c + 4\gamma_2^2 d + 10\gamma_2^4 e, \quad (\text{A15})$$

where $\vec{\epsilon}_{(\gamma)}^*$ is the polarization vector of the outgoing photon, \hat{k}' is the unit vector of the photon three-momentum, and \hat{p} is the unit vector of the relative momentum of the initial α - ^{12}C system. The amplitude $X^{(l=2)}$ is decomposed as

$$X^{(l=2)} = X_{(a+b)}^{(l=2)} + X_{(c)}^{(l=2)} + X_{(d+e)}^{(l=2)} + X_{(f)}^{(l=2)}, \quad (\text{B2})$$

where each amplitude corresponds to the diagrams depicted in Fig. B1. Thus, we have

$$X_{(a+b)}^{(l=2)} = -6y^{(0)} e^{i\sigma_2} \Gamma(1 + \kappa/\gamma_0) \int_0^\infty dr r W_{-\kappa/\gamma_0, \frac{1}{2}}(2\gamma_0 r) \left[\frac{Z_\alpha \mu}{m_\alpha} j_1 \left(\frac{\mu}{m_\alpha} k' r \right) + \frac{Z_C \mu}{m_C} j_1 \left(\frac{\mu}{m_C} k' r \right) \right] \left(\frac{\partial}{\partial r} + \frac{3}{r} \right) \frac{F_2(\eta, pr)}{pr}, \quad (\text{B3})$$

$$X_{(c)}^{(l=2)} = +y^{(0)} \left\{ -h_R^{(2)} + \frac{3\kappa\mu^3 m_O^2}{2\pi Z_O} \left(\frac{Z_\alpha}{m_\alpha^2} + \frac{Z_C}{m_C^2} \right) \left[\frac{4}{225} \ln \left(\frac{\mu_{DR}}{2} r_C \right) - \ln \left(\frac{\mu_{DR}}{\kappa} \right) \right] \right\} \frac{5\pi Z_O e^{i\sigma_2} k' p^2 \sqrt{(1+\eta^2)(4+\eta^2)} C_\eta}{\mu m_O^2 K_2(p) - 2\kappa H_2(p)}, \quad (\text{B4})$$

$$X_{(d+e)}^{(l=2)} = +\frac{1}{5} y^{(0)} \frac{e^{i\sigma_2} p^4 \sqrt{(1+\eta^2)(4+\eta^2)} C_\eta}{K_2(p) - 2\kappa H_2(p)} \Gamma(1 + \kappa/\gamma_0) \Gamma(3 + i\eta) \int_{r_C}^\infty dr r W_{-\kappa/\gamma_0, \frac{1}{2}}(2\gamma_0 r) \left[\frac{Z_\alpha \mu}{m_\alpha} j_1 \left(\frac{\mu}{m_\alpha} k' r \right) + \frac{Z_C \mu}{m_C} j_1 \left(\frac{\mu}{m_C} k' r \right) \right] \left(\frac{\partial}{\partial r} + \frac{3}{r} \right) \frac{W_{-i\eta, \frac{5}{2}}(-2ipr)}{r}, \quad (\text{B5})$$

$$X_{(f)}^{(l=2)} = -\frac{15}{4} y^{(0)} \mu^2 \left(\frac{Z_\alpha}{m_\alpha^2} + \frac{Z_C}{m_C^2} \right) [-2\kappa H(\eta_{0b})] \frac{e^{i\sigma_2} k' p^2 \sqrt{(1+\eta^2)(4+\eta^2)} C_\eta}{K_2(p) - 2\kappa H_2(p)}, \quad (\text{B6})$$

where m_α , m_C , and m_O (Z_α , Z_C , and Z_O) are the masses

(numbers of protons) of α , ^{12}C , and ^{16}O , respectively; μ

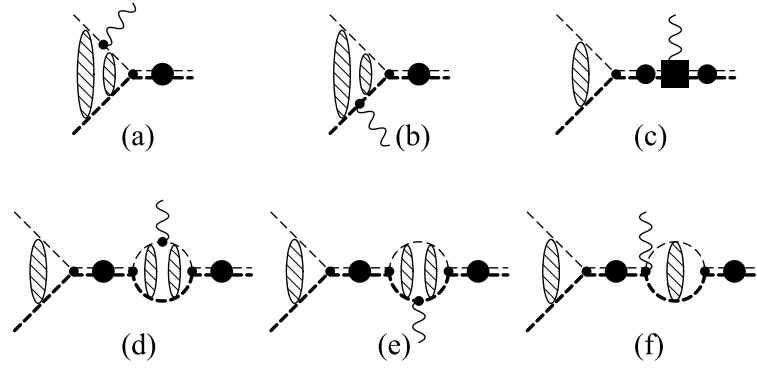


Fig. B1. Diagrams of amplitudes for radiative α capture on ^{12}C . The wavy and thin (thick) dashed lines denote the outgoing photon and α (^{12}C) state, respectively. The double thin-and-thick lines with a filled circle denote the dressed ^{16}O propagators for the 2_1^+ state in the intermediate state and for the 0_1^+ state in the final state. Please, refer also to the caption in Fig. 1. The $O\gamma O^*$ vertex in diagram (c) is a counter term proportional to $h_R^{(2)}$ to renormalize the infinities from loop diagrams in (d), (e), and (f).

and κ are the reduced mass and the inverse of the Boer radius of the α - ^{12}C system; k' and p are the magnitude of the three momentum of the outgoing photon and that of the relative momentum of the α - ^{12}C system in the center-of-mass frame; η is the Sommerfeld parameter, $\eta = \kappa/p$; γ_0 is the binding momentum of the ground state of ^{16}O , with $\gamma_0 = \sqrt{2\mu B_0}$, where B_0 is the binding energy of the α - ^{12}C system in the ground state of ^{16}O ; and $\eta_{0b} = \kappa/(i\gamma_0)$. $\Gamma(z)$, $j_l(x)$, $F_l(\eta, \rho)$, and $W_{\kappa, \mu}(z)$ are the gamma, spherical Bessel, regular Coulomb, and Whittaker functions, respectively; σ_2 is the Coulomb phase shift for $l = 2$.

The three loop diagrams of the $O\gamma O^*$ vertex in Figs. B1(d), (e), and (f) diverge. The log divergence appears in the r -space integral at the $r \rightarrow 0$ limit in Eq. (52) for diagrams (d) and (e); we introduce a cutoff r_c in the r -space integral and the infinite part is renormalized by the counter term $h^{(2)}$ in Eq. (51). The divergence appearing in diagram (f) was regulated in the momentum space integral as J_0^{div} by means of dimensional regularization [49, 50]. Those infinities are renormalized by the renormalized coefficient $h_R^{(2)}$ as

$$\begin{aligned} & -h^{(2)} + \frac{3\mu^2 m_O^2}{2Z_O} \left(\frac{Z_\alpha}{m_\alpha^2} + \frac{Z_C}{m_C^2} \right) \\ & \left[-J_0^{div} + \frac{4\kappa\mu}{225\pi} \left(\frac{\mu_{DR}}{2} \right)^{2\epsilon} \int_0^{r_c} \frac{dr}{r^{1-2\epsilon}} \right] \\ & = -h_R^{(2)} + \frac{3\kappa\mu^3 m_O^2}{2\pi Z_O} \left(\frac{Z_\alpha}{m_\alpha^2} + \frac{Z_C}{m_C^2} \right) \\ & \left[-\ln \left(\frac{\mu_{DR}}{\kappa} \right) + \frac{4}{225} \ln \left(\frac{\mu_{DR}}{2} r_c \right) + O(\epsilon) \right], \end{aligned} \quad (\text{B7})$$

with

$$J_0^{div} = \frac{\mu\kappa}{2\pi} \left[\frac{1}{\epsilon} - 3C_E + 2 + \ln \left(\frac{\pi\mu_{DR}^2}{4\kappa^2} \right) \right], \quad (\text{B8})$$

where we performed the integration in $d = 4 - 2\epsilon$ dimensions, μ_{DR} is the scale of dimensional regularization, and C_E is Euler's constant, $C_E = 0.5771 \dots$; we set $\mu_{DR} = \Lambda_H = 160$ MeV. We found a minor cutoff r_c dependence and set $r_c = 0.01$ fm. The $E2$ transition amplitudes up to this order have two additional parameters, $h_R^{(2)}$ and $y^{(0)}$, along with the effective range parameters, r_2 , P_2 , and Q_2 , in the function of $K_2(p)$.

The total cross-section is expressed as

$$\sigma_{E2} = \frac{4}{3} \frac{\alpha_E \mu E'_\gamma}{p(1 + E'_\gamma/m_O)} \frac{1}{5} |X^{(l=2)}|^2, \quad (\text{B9})$$

where $E'_\gamma (= k')$ is the energy of the outgoing photon,

$$E'_\gamma \simeq B_0 + E - \frac{1}{2m_O} (B_0 + E)^2, \quad (\text{B10})$$

and the S_{E2} factor is defined as

$$S_{E2}(E) = \sigma_{E2}(E) E e^{2\pi\eta}. \quad (\text{B11})$$

References

- [1] W. A. Fowler, *Rev. Mod. Phys.* **56**, 149 (1984)
- [2] T. A. Weaver and S. E. Woosley, *Phys. Rep.* **227**, 65 (1993)
- [3] G. Imbriani *et al.*, *Astr. Jour.* **558**, 903 (2001)
- [4] J. José, *Stellar Explosions, Hydrodynamics and Nucleosynthesis*, (CRC Press, first issued in paperback 2020)

- [5] D. R. Tilley, H. R. Weller, and C. M. Cheves, *Nucl. Phys. A* **564**, 1 (1993)
- [6] L. R. Buchmann and C. A. Barnes, *Nucl. Phys. A* **777**, 254 (2006)
- [7] A. Coc *et al.*, *Eur. Phys. J. A* **51**, 34 (2015)
- [8] C. A. Bertulani and T. Kajino, *Prog. Part. Nucl. Phys.* **89**, 56 (2016)
- [9] R. J. deBoer *et al.*, *Rev. Mod. Phys.* **89**, 035007 (2017)
- [10] S. I. Ando, *Eur. Phys. J. A* **57**, 17 (2021)
- [11] S. I. Ando, *J. Hyoj. Acad.* **1**, 41 (2023)
- [12] S. Weinberg, *Physica A* **96**, 327 (1979)
- [13] H. W. Hammer, S. König, and U. van Kolck, *Rev. Mod. Phys.* **92**, 025004 (2020)
- [14] J. F. Donoghue, E. Golowich, and B. R. Holstein, *Dynamics of the Standard Model* (Second Edition, Cambridge University Press, 2014)
- [15] E. J. In, T. S. Park, Y. H. Song *et al.*, *Phys. Rev. C* **109**, 054622 (2024)
- [16] F. Nazari, M. Radin, and M. M. Arani, *Eur. Phys. J. A* **59**, 20 (2023)
- [17] S. Son, S. I. Ando, and Y. Oh, *New Phys.:Sae Mulli* **72**, 291 (2022)
- [18] S. Son, S. I. Ando, and Y. Oh, *Phys. Rev. C* **106**, 055807 (2022)
- [19] S. I. Ando, *Eur. Phys. J. A* **52**, 130 (2016)
- [20] S. I. Ando, *Phys. Rev. C* **97**, 014604 (2018)
- [21] S. I. Ando, *J. Korean Phys. Soc.* **73**, 1452 (2018)
- [22] S. I. Ando, *Phys. Rev. C* **105**, 064603 (2022)
- [23] S. I. Ando, *Phys. Rev. C* **107**, 045808 (2023)
- [24] S. I. Ando, *Phys. Rev. C* **100**, 015807 (2019)
- [25] P. Tischhauser *et al.*, *Phys. Rev. C* **79**, 055803 (2009)
- [26] S. König, D. Lee, and H. W. Hammer, *J. Phys. G: Nucl. Part. Phys.* **40**, 045106 (2013)
- [27] C. R. Brune *et al.*, *Phys. Rev. Lett.* **83**, 4025 (1999)
- [28] J. M. Sparenberg, P. Capel, and D. Baye, *J. Phys.: Conf. Seri.* **312**, 082040 (2011)
- [29] S. I. Ando, *Few-Body Syst.* **65**, 7 (2024)
- [30] M. D'Agostino Bruno, I. Massa, A. Uguzzont *et al.*, *Il Nuovo Cimento* **27**, 1 (1975)
- [31] A. M. Mukhamedzhanov *et al.*, *Phys. Rev. C* **110**, 055803 (2024)
- [32] J. Gasser, M. E. Sainio, and Švarc, *Nucl. Phys. B* **307**, 779 (1988)
- [33] S. I. Ando and H. W. Fearing, *Phys. Rev. D* **75**, 014025 (2007)
- [34] Z. R. Iwinski, L. Rosenberg, and L. Spruch, *Phys. Rev. C* **29**, 349 (1984)
- [35] D. Foreman-Mackey *et al.*, *Jour. Open Sour. Soft.* **14**, 1864 (2019)
- [36] R. J. deBoer *et al.*, *Phys. Rev. C* **85**, 045804 (2012)
- [37] J. M. L. Ouellet *et al.*, *Phys. Rev. C* **54**, 1982 (1996)
- [38] G. Roters, C. Rolfs, F. Strieder *et al.*, *Eur. Phys. J. A* **6**, 451 (1999)
- [39] R. Kunz *et al.*, *Phys. Rev. Lett.* **86**, 3244 (2001)
- [40] M. Fey, *Im Brennpunkt der Nuklearen Astrophysik: Die Reaktion $^{12}\text{C}(\alpha, \gamma)^{16}\text{O}$* , Ph. D thesis (Universität Stuttgart, 2004)
- [41] H. Makii *et al.*, *Phys. Rev. C* **80**, 065802 (2009)
- [42] R. Plag *et al.*, *Phys. Rev. C* **86**, 015805 (2012)
- [43] H. Poincaré, *La Science et L'Hypothese*, (1902), (Japanese translation, translated by I. Khono, Iwanami Bunko (2020))
- [44] M. L. Avila *et al.*, *Phys. Rev. Lett.* **114**, 071101 (2015)
- [45] C. Hebborn, M. L. Avila, K. Kravvaris *et al.*, *Phys. Rev. C* **109**, L061601 (2024)
- [46] C. Hebborn, G. Hupin, K. Kravvaris *et al.*, *Phys. Rev. Lett.* **129**, 042503 (2022)
- [47] M. Abramowitz and I. A. Stegun, *Handbook of mathematical functions with formulas, graphs, and mathematical tables*, (Martino Publishing, Mansfield Center, CT, 2014)
- [48] F. W. J. Olver, D. W. Lozier, R. F. Boisvert *et al.*, *NIST Handbook of Mathematical Functions*, (Cambridge University Press, 2010)
- [49] X. Kong and F. Ravndal, *Phys. Lett. B* **450**, 320 (1999)
- [50] S. I. Ando, J. W. Shin, C. H. Hyun *et al.*, *Phys. Rev. C* **76**, 064001 (2007)